INL/RPT-XX-XXXXX

Modeling Heat Pipes with Non-Condensable Gases

August 2023

Mauricio Tano[1], Piyush Sabharwall[1], and Katrina Sweetland[2]

[1]*Idaho National Laboratory*
[2]*Los Alamos National Laboratory*

Idaho National Laboratory

INL is a U.S. Department of Energy National Laboratory
operated by Battelle Energy Alliance, LLC

INL/RPT-XX-XXXXX

Modeling Heat Pipes with Non-Condensable Gases

Mauricio Tano[1], Piyush Sabharwall[1], and Katrina Sweetland[2]

[1]**Idaho National Laboratory**
[2]**Los Alamos National Laboratory**

August 2023

Idaho National Laboratory
Idaho Falls, Idaho 83415

http://www.inl.gov

Prepared for the
U.S. Department of Energy
Office of _____
Under DOE Idaho Operations Office
Contract DE-AC07-05ID14517

Page intentionally left blank

ABSTRACT

The subsequent report showcases advancements in modeling heat pipes, considering both scenarios with and without non-condensable gases. To achieve this, two distinct modeling approaches are juxtaposed. Firstly, the effective conduction model, implemented in the MOOSE-based code Sockeye, is employed. Secondly, a first-of-a-kind two-phase Euler-Euler Computational Fluid Dynamics (CFD) model is developed using the STAR-CCM+ code. Both models undergo validation against experimental data, acknowledging the inherent uncertainties associated with each modeling assumption. Interestingly, the non-tuned CFD model surpasses the performance of the calibrated conduction model for heat pipes operating under both conditions: with and without non-condensable gases. It's worth noting, however, that the CFD models entail significantly longer runtimes compared to the conduction models. Nevertheless, the insights garnered from the CFD model shed invaluable light on the intricate operational dynamics of heat pipes. Future work involves broadening the validation scope of these models and continuing their development to enhance their utility as robust tools for heat pipe design and operational support.

Page intentionally left blank

CONTENTS

FIGURES

TABLES

Page intentionally left blank

1. Introduction

Heat pipes serve as highly effective heat transfer devices widely employed across various industries for thermal management and cooling applications. Their remarkable heat transfer capabilities stem from phase change phenomena involving evaporation and condensation within a confined system. However, the presence of non-condensable gases within heat pipes can significantly influence their thermal performance and overall operation. This report delves into the effects of non-condensable gases on heat pipe operations, highlighting the imperative of incorporating their behavior into numerical simulations for precise modeling. We investigate two separate models.

The investigation revolves around two models designed to account for the impact of non-condensable gases. First, an effective heat conduction model is explored, which characterizes heat conduction through the heat pipe by using an effective thermal conductivity for the core and wick of the heat pipe at the evaporator and condenser segments. Second, a novel multi-phase Euler-Euler Computational Fluid Dynamics (CFD) model is introduced. This model aims to accurately capture mass, momentum, and energy conservation in heat pipes, offering deeper insights into their behavior. Both models are compared against experimental data from a water-copper heat pipe operating with single evaporator and condenser configurations, with and without non-condensable gases.

Non-condensable gases, such as air or inert gases, are molecules incapable of undergoing phase change within the heat pipe's specific temperature and pressure ranges. Their presence have multiple advantages of operarting heat pipes with non-condensable gases. The main ones are listed here below:

Non-condensable gases, such as helium or nitrogen, are sometimes intentionally introduced into heat pipes for specific engineering reasons. The advantages of having non-condensable gases in a heat pipe include:

Thermal Resistance Adjustment: Non-condensable gases can be used to adjust the overall thermal resistance of the heat pipe. By controlling the amount of non-condensable gas, engineers can fine-tune the thermal performance of the heat pipe to meet specific requirements.

Lower Operating Temperatures: The presence of non-condensable gases can increase the

operating temperature range of the heat pipe. This can be useful in applications where the heat source or heat sink temperatures vary widely.

Improved Startup and Restart: Non-condensable gases can assist in the startup and restart of a heat pipe. They help to prevent the formation of vapor locks and ensure that the heat pipe begins functioning efficiently even in challenging conditions.

Enhanced Heat Transfer Control: Non-condensable gases can be used to control and stabilize heat transfer within the heat pipe. This is especially important in situations where rapid changes in temperature or heat load occur.

Reduced Corrosion and Erosion: The presence of non-condensable gases can help reduce the risk of corrosion and erosion within the heat pipe. This can extend the operational lifespan of the heat pipe.

Resistance to Gravity Effects: In some applications, non-condensable gases can help mitigate the adverse effects of gravity on heat pipe performance. This is important for heat pipes used in various orientations, such as in space applications.

Improved Compatibility with Working Fluids: Non-condensable gases can be used to tailor the compatibility of the heat pipe with specific working fluids, which can be important in environments with aggressive chemicals.

It's important to note that the use of non-condensable gases in a heat pipe is a design choice that depends on the specific requirements of the application. Engineers carefully consider factors such as heat load, temperature range, orientation, and materials compatibility when deciding whether to incorporate non-condensable gases into a heat pipe design. However, in the operation of the heat pipe, several challenges may be associated to the operation of the heat pipe with non-condensable gases that disrupts smooth heat pipe operation. These limitations are related to bubbles of gas occupying the wick structure of the heat pipe and influencing the mass flow rates of the working fluid. Consequently, modeling and operational challenges emerge. A few ones are listed here below.

Reduced Effective Length: Non-condensable gases limit the effective length available for vapor flow, obstructing heat transfer. Extended heat pipes are particularly vulnerable, as accumulation of non-condensable gases can diminish effective length and compromise device performance.

Thermal Resistance: These gases act as thermal insulators, reducing the effective thermal conductivity of the working fluid. This results in increased thermal resistance and diminished heat transfer rate, ultimately undermining the heat pipe's heat dissipation efficiency.

Pressure Drop: Non-condensable gases contribute to additional pressure drop along the vapor flow path, affecting fluid dynamics. This pressure drop can impede vapor flow, leading to uneven temperature distribution and potential hot spots.

Startup and Restart Challenges: Non-condensable gases pose challenges during heat pipe startup and restart. Accumulation at specific points can hinder proper priming and initiation of the phase change cycle and cause the accumulation of non-condensable gases in the liquid path, affecting steady-state operation.

To accurately predict heat pipe behavior in the presence of non-condensable gases, their inclusion in numerical simulations becomes essential. Traditional models that solely focus on working fluid behavior might not capture intricate interactions between the working fluid and non-condensable gases. Several approaches address this:

Two-Fluid Models: These models differentiate between working fluid and non-condensable gas behavior, tracking both flows separately to offer insights into how non-condensable gases influence fluid dynamics and heat transfer. Our models do not yet consider mass transfer by diffusion between the vapor and non-condensable gas phase, which have been observed in practice.

Mass and Momentum Equations: Incorporating mass and momentum equations for non-condensable gases enhances simulation accuracy, considering pressure drop, velocity distribution, and the entrainment of non-condensable gases by vapor flow.

Multiphysics Simulations: Multiphysics simulations combine heat transfer, fluid dynamics, and mass transport to comprehensively model heat pipe behavior with non-condensable gases. Such simulations provide comprehensive insights into system responses under varying conditions.

Accurate modeling of non-condensable gases within heat pipes is essential for several reasons:

Performance Optimization: Precise simulations empower engineers to optimize heat pipe designs by accounting for non-condensable gas effects, leading to improved thermal performance and heightened efficiency.

Enhanced Reliability: Understanding the impact of non-condensable gases aids in predicting performance degradation, preventing failures, and ensuring reliable operation throughout the heat pipe's operational lifespan.

Customization and Adaptation: Accurate modeling facilitates the customization of heat pipes for specific conditions, enabling tailored solutions for diverse environments.

Accurate numerical simulations are pivotal for comprehending their behavior and interactions with the working fluid. Such modeling aids in designing and optimizing heat pipes for various applications while ensuring reliability and efficiency. As research progresses, addressing the effects of non-condensable gases becomes crucial to advancing heat pipe capabilities and expanding their potential in modern thermal management systems.

The presence of non-condensable gases in heat pipes introduces complexities that warrant in-depth investigation. Theoretical and numerical modeling approaches have played a pivotal role in understanding the intricate interplay between the working fluid and non-condensable gases within these systems.

Numerous studies have been conducted to elucidate the behavior of heat pipes with non-condensable gases.

C.L. Tien conducted experiments and modeling. In 1973, A.R. Rohani and C.L. Tien [1] performed a simple lumped-parameters 2D numerical analysis of heat and mass transfer in variable conductance heat pipes, neglecting axial conduction, liquid-filled wick effects, and interaction between the liquid, vapor, and gases across the pipe core and wick interface. Two dimensionless parameters were introduced: one comparing axial thermal energy transfer to conduction, and the other comparing energy transferred by diffusion to conduction. Six cases were tested, varying vapor-gas mixture, heat pipe diameter, initial vapor temperature, and ambient temperature. Different non-dimensional parameter values were obtained, indicating heat pipe performance dependence on physical parameters and the significance of gas-vapor energy and mass transfer.

Prado-Monte et al. [2] employed a comprehensive homogeneous model to simulate heat pipe behavior under the influence of non-condensable gases. Their model captured the distinct dynamics of the working fluid and non-condensable gases, shedding light on the intricate interactions between these two phases. This approach aligns with the homogeneous flow theory

that underpins the fundamental understanding of heat pipe operation.

The work by Huang et al. [3] further expanded on this foundation by augmenting the traditional one-dimensional heat pipe model with more comprehensive mass and momentum equations for non-condensable gases. This inclusion aligned with the concept of multiphase flow and enabled a more accurate representation of pressure drop, entrainment, and velocity distribution within the heat pipe. Their work not only emphasized the importance of capturing these phenomena but also demonstrated how they are interconnected, echoing the principles of fluid dynamics.

While not specific to heat pipes, Lee et al. [4] ventured into coupling heat transfer, fluid dynamics, and mass transport phenomena for condensing liquids. By intertwining these intricate factors, they holistically portrayed the behavior of non-condensable gases during condensation. This integration resonates with the philosophy of understanding complex systems by considering the synergistic effects of multiple physical processes. Kekaula et al. [5] further expanded on these studies by developing a more detailed multidimensional model of steam condensation in the presence of non-condensable gases, showcasing the capabilities of modern computational CFD tools in predicting the mechanical interaction of condensing vapor and non-condensable gases.

A few recent CFD studies have been conducted for heat pipes using liquid metals. For instance, Sun et al. [6] successfully employed a homogenized CFD model to study the operation of a potassium heat pipe at various inclination angles. Additionally, Wang et al. [7] recently used a mixture CFD model to demonstrate hydrogen inactivation in a liquid metal heat pipe. However, in these cases, the high thermal conductivity of liquid metals helps homogenize the thermal conductivity on the liquid-vapor interfaces, yielding appropriate homogeneous models for simulation purposes. However, for the more general case of a liquid and vapor operating with markedly different thermophysical properties, a homogeneous CFD model yields diffusive results that may not properly represent the operational behavior of the heat pipe.

This work advances upon prior efforts by demonstrating the application of a two-phase Euler-Euler CFD model for heat pipes. The modeling approach's details are presented in this report, along with the implemented mass, momentum, and energy closure models. Furthermore, the model is extended to account for the presence of non-condensable gases. We validate this model against experimental data and demonstrate its capability to outperform the standard effective

conduction model used for heat pipes without the need for tuning.

2. Codes and Code Jargon

The focus of this work is the validation of heat pipe models against experimental data. These models are developed using the following codes:

- MOOSE: MOOSE (Multiphysics Object-Oriented Simulation Environment) is an open-source finite element framework developed by Idaho National Laboratory (INL) for solving complex multiphysics and multiscale problems. MOOSE provides a flexible and extensible platform for solving coupled systems of partial differential equations (PDEs) arising in a wide range of scientific and engineering applications. It allows researchers and engineers to build custom simulations that involve multiple physical phenomena, such as heat transfer, fluid flow, chemical reactions, and more, all within a unified framework.

- Sockeye: It is MOOSE heat pipe modeling module. The code has been under development during several years and currently supports different modeling methods for heat pipes. The most developed model in Sockeye is the conduction model, which is tested in this report, while the vapor-only and two-phase 1D models are more immature in its development.

- STAR-CCM+: STAR-CCM+ is a computational fluid dynamics (CFD) software developed by Siemens Digital Industries Software that enables engineers and researchers to simulate and analyze complex fluid flow, heat transfer, and related physics phenomena. Known for its user-friendly interface and powerful simulation capabilities, STAR-CCM+ provides pre-processing, solving, and post-processing tools in an integrated environment. Although the STAR-CCM+ code is note opened, one can extend its models and code through its Java-based scripting language, which allows users to customize simulations, create new physics models, and implement specialized algorithms. This scripting capability enables users to tailor simulations to specific needs, automate repetitive tasks, develop new turbulence models, integrate user-defined boundary conditions, and even couple CFD simulations with other engineering disciplines, contributing to the software's adaptability and versatility for diverse engineering applications.

3. Theory

As previously mentioned, two models are compared for modeling heat pipes with and without non-condensable gases. On the one hand, a simple conduction model implemented in Sockeye, which is intended to provide fast estimates to the heat exchange behaviour in the heat pipe. This model is implemented in Sockeye. On the other hand, a more refined two-phase with non-condensables CFD model that is implemented in STAR-CCM+. The goal of this model is to provide further numerical insights into the behaviour of the heat pipes but is not intended for multiscale coupling at a reactor scale like Sockeye.

3.1 Sockeye Conduction Model

In this section, we describe the conduction model implemented in Sockeye for modeling the heat pipe. Further references and descriptions can be found in the code's documentation.

3.1.1 Heat Pipe Modeling using Effective Heat Conduction

The Conduction Model presents a pragmatic and robust approach as an alternative to the more intricate Flow Model. In this model, a heat pipe is conceptually approximated as a solid rod endowed with an extraordinarily high thermal conductivity. Rather than grappling with the complexities of solving two-phase flow equations within the heat pipe's interior, the Conduction Model leverages heat conduction equations throughout the entire structure—spanning the vapor core, wick, and cladding. This strategy ingeniously captures thermal-hydraulic interactions by adroitly defining thermal properties and/or boundary conditions.

3.1.2 Governing Equations for the Conduction Modeling

The crux of the conduction heat pipe model lies within the transient heat conduction equation:

$$\rho c \frac{\partial T}{\partial t} - \nabla \cdot (k \nabla T) = q''' \tag{1}$$

In this equation:

- $T(\mathbf{x}, t)$ represents the temperature,

- ρ denotes the density (assumed constant),
- c signifies the specific heat capacity (assumed constant),
- $k(T)$ accounts for thermal conductivity (dependent on temperature), and
- $q'''(\mathbf{x}, t)$ embodies the volumetric heat source.

Typically, the Conduction Model classifies three distinct subdomains:

Subdomain	Spatial Range	Description
Ω_{core}	$r \leq R_{\text{wick,i}}$	Vapor core
$\Omega_{\text{wick-ann}}$	$R_{\text{wick,i}} < r \leq R_{\text{clad,i}}$	Wick and annulus
Ω_{clad}	$R_{\text{clad,i}} < r \leq R_{\text{clad,o}}$	Cladding

It is noteworthy that $\Omega_{\text{wick-ann}}$ could be further subdivided into distinct subdomains for the wick and annulus.

Each subdomain is characterized by distinct formulations for thermal properties ρ, c, and k. For the cladding, these properties are straightforwardly derived from the equation of state for the cladding material. Concerning the wick/annulus, a weighted average approach is adopted, encompassing liquid and wick material properties. For the vapor core, density and specific heat capacity are attributed values corresponding to vapor properties. However, the thermal conductivity is a dynamically controlled function of time, aimed at emulating heat pipe performance. This synopsis is succinctly tabulated, with p_{sat} representing the working fluid saturation pressure at temperature T:

Subdomain	ρ	c	k
Ω_{core}	$\rho_v(p_{\text{sat}}, T)$	$c_{p,v}(p_{\text{sat}}, T)$	$k_{\text{core}}(t)$
$\Omega_{\text{wick-ann}}$	$\bar{\rho}(\rho_\ell(p_{\text{sat}}, T), \rho_w(T))$	$\bar{c}(c_{p,\ell}(p_{\text{sat}}, T), c_w(T))$	$\bar{k}(k_\ell(p_{\text{sat}}, T), k_w(T))$
Ω_{clad}	$\rho_{\text{clad}}(T)$	$c_{\text{clad}}(T)$	$k_{\text{clad}}(T)$

3.1.3 Core Thermal Conductivity Control

Central to this model is the orchestrated management of core thermal conductivity, denoted as $k_{\text{core}}(t)$. This pivotal control mechanism invokes analytic heat pipe limit relations, encompassing

capillarity, boiling, entrainment, viscosity, and sonic operational limits. These limits, each expressed as functions of temperature $\dot{Q}_i(T)$, serve to govern heat transfer within the vapor core. Should heat transfer across a surface transgress a predefined limit, the core's thermal conductivity is proportionally attenuated until compliance is restored. Typically, the surface chosen for heat rate measurement is the evaporator exit within the vapor core:

$$\dot{Q} = \int_{A_{\text{evap,exit}}} -k \frac{\partial T}{\partial x} dA \tag{2}$$

$$A_{\text{evap,exit}} \equiv \{\mathbf{x} : x = x_{\text{evap,exit}}, r \leq R_{\text{wick,i}}\} \tag{3}$$

Evaluation of these limits is conducted at a reference temperature T_{ref}, often derived from the solution itself, such as the evaporator end cap temperature—ideal for the sonic limit. Alternatively, each limit can be evaluated at its own distinct reference temperature. Some limits are identified as "catastrophic failure" limits, indicated as $\dot{Q}_i^{\text{cat}}$. Breaching these limits leads to heat pipe failure for the remaining transient period. Such failure triggers entail setting the core's thermal conductivity to a predetermined minimum value $k_{\text{core,min}}$ for the duration of the transient. These catastrophic failure limits usually pertain to dryout scenarios, such as the capillary, entrainment, and boiling limits.

On the contrary, other limits are characterized as transient "recoverable" limits, termed $\dot{Q}_i^{\text{rec}}$, often applied to viscous and sonic limits. These limits ensure that the core's thermal conductivity is adjusted proportionally to sustain compliance:

$$k_{\text{core}}^{n+1} = \gamma k_{\text{core}}^{n} \tag{4}$$

$$\gamma = \frac{\min_i(\dot{Q}_i^{\text{rec}}(T_{\text{ref}}^n))}{\dot{Q}^n} \tag{5}$$

Here, n denotes the time step index.

3.1.4 Modeling Non-Condensable Gases in the Conduction Model

The presence of non-condensable gases (NCGs) introduces a distinctive element influencing heat pipe behavior. NCGs tend to accumulate at the condenser's end, effectively curtailing the active condenser length and impeding the condensation of the working fluid. A rudimentary model to account for NCGs involves assigning a low thermal conductivity, $k_{\text{core},i}$, to the inactive length of the heat pipe, and a high thermal conductivity, $k_{\text{core},a}$, to the active length:

$$k_{\text{core}} = \begin{cases} k_{\text{core},a} & x \leq x_{\text{front}} \\ k_{\text{core},i} & x > x_{\text{front}} \end{cases} \tag{6}$$

Here, $x \leq x_{\text{front}}$ pertains to the active length, with x_{front} representing the front position of the NCG portion.

The steady flat-front model of NCGs approximates the interface between the working fluid and NCGs as a discontinuous jump, departing from the smoother transition observed in reality due to mass diffusion. Adhering to Dalton's law of partial pressures, the total pressure of a gas mixture equals the sum of partial pressures. Balancing pressures at the interface yields the NCG partial pressure as a function of partial vapor pressures on either side of the interface:

$$p_{g,i} = p_{v,a} - p_{v,i} \tag{7}$$

Here:

- $p_{g,i}$ denotes the NCG pressure in the inactive length of the condenser,
- $p_{v,a}$ signifies the vapor pressure in the active length of the condenser, and
- $p_{v,i}$ represents the vapor pressure in the inactive length of the condenser.

The mass of NCG is calculated as $m_g = \rho_g A_v L_{c,i}$, where:

- ρ_g stands for the density of the gas,
- A_v denotes the vapor core cross-sectional area, and
- $L_{c,i}$ signifies the inactive length of the condenser.

Application of the ideal gas law to the NCG leads to the expression of the inactive length as a function of pressures and temperatures:

$$L_{c,i} = \frac{m_g R_g T_{g,i}}{p_{g,i} A_v} \tag{8}$$

In this context:

- R_g represents the specific gas constant of the NCG, and
- $T_{g,i}$ denotes the temperature of the inactive length.

This methodology necessitates the determination of temperatures to assess active and inactive length pressures. Let T_{hot} denote the active length temperature, facilitating the evaluation of vapor pressure in the active length: $p_{v,a} = p_{v,\text{sat}}(T_{\text{hot}})$. Let T_{cold} signify the inactive length temperature, serving to determine the inactive length vapor pressure: $p_{v,i} = p_{v,\text{sat}}(T_{\text{cold}})$, and $T_{g,i} = T_{\text{cold}}$. In practice, these temperatures can be approximated using the maximum and minimum temperatures, yielding T_{hot} and T_{cold} respectively.

3.2 Multiphase flow modeling in the heat pipe

Mixture models have been recently used to simulate the two-phase flow behaviour in heat pipes. However, these models present several limitations. First, closures terms must be introduced to guarantee the correct behaviour of momentum and mass transfer at the liquid-vapor interfaces. These exchange coefficients often depend on the thermal and configuration of the flow regime. Second, the mixture models are over-diffusive. This lead to only approximated predictions of the flow dynamics within the heat pipe. Finally, mixture models cannot appropriately capture compressibility effects in the gaseous phase of the heat pipe and hence, can lead to an incorrect behaviour of the gas dynamics as the jet of generated vapor expands and accelerate at the evaporator and stop and decelerate at the condenser.

Two-phase flows are common in various industrial processes, ranging from chemical engineering to nuclear power generation. The Euler-Euler approach in Computational Fluid Dynamics (CFD) is a widely used technique to simulate such flows. In this model, both phases are treated as continuous fluid phases with distinct properties and the momentum and thermal

equilibrium at the interface between both faces is resolved via mechanistic interface models. Additionally, the independent treatment of both phases allows us to integrate compressible gas dynamics into the vapor phase. In the next paragraphs, we provide a broad description of the two-phase Euler-Euler models, their governing equations, closure relations, energy conservation equations, and the integration of the modeling of non-condensable gases. The section is not meant to be extensive but rather to give an overview of the models solved and describes its particularities when applied to heat pipes. The equations are described generically for two phases 1 and 2, understanding that in this work phase 1 will be the liquid water phase and phase 2 will be the water vapor.

The two-phase Euler-Euler approach involves solving the mass and momentum conservation equations for both phases separately. The governing equations for each phase can be summarized as follows:

Mass Conservation for Phase 1:

$$\frac{\partial \rho_1}{\partial t} + \nabla \cdot (\rho_1 \mathbf{u}_1) = -\dot{\rho}_{\text{evap}} + \dot{\rho}_{\text{cond}} \tag{9}$$

Momentum Conservation for Phase 1:

$$\frac{\partial (\rho_1 \mathbf{u}_1)}{\partial t} + \nabla \cdot (\rho_1 \mathbf{u}_1 \mathbf{u}_1) = -\nabla p_1 + \nabla \cdot \tau_1 + \rho_1 \mathbf{g} + \mathbf{F}_{\text{drag,1-2}} \tag{10}$$

Energy Conservation for Phase 1:

$$\frac{\partial}{\partial t}(\rho_1 e_1) + \nabla \cdot (\rho_1 e_1 \mathbf{u}_1) = -\nabla \cdot \mathbf{q}_1 + \rho_1 \dot{q}_{\text{evap,1}} + \rho_1 \dot{q}_{\text{cond,1}} \tag{11}$$

Where:

ρ_1 : Density of Phase 1

$\mathbf{u}_1$: Velocity of Phase 1

p_1 : Pressure of Phase 1

τ_1 : Stress tensor of Phase 1

$\mathbf{g}$: Gravitational acceleration

$\mathbf{F}_{\text{drag,1-2}}$: Drag force on Phase 1 due to Phase 2

e_1 : Internal energy of Phase 1

$\mathbf{q}_1$: Heat flux in Phase 1

$\dot{q}_{\text{evap,1}}$: Evaporation heat transfer rate in Phase 1

$\dot{q}_{\text{cond,1}}$: Condensation heat transfer rate in Phase 1

$\dot{\rho}_{\text{evap,1}}$: Evaporation mass transfer of Phase 1

$\dot{\rho}_{\text{cond,1}}$: Condensation mass transfer rate in Phase 2

Mass Conservation for Phase 2:

$$\frac{\partial \rho_2}{\partial t} + \nabla \cdot (\rho_2 \mathbf{u}_2) = \dot{\rho}_{\text{evap}} - \dot{\rho}_{\text{cond}} \tag{12}$$

Momentum Conservation for Phase 2:

$$\frac{\partial (\rho_2 \mathbf{u}_2)}{\partial t} + \nabla \cdot (\rho_2 \mathbf{u}_2 \mathbf{u}_2) = -\nabla p_2 + \nabla \cdot \tau_2 + \rho_2 \mathbf{g} + \mathbf{F}_{\text{drag,2-1}} \tag{13}$$

Energy Conservation for Phase 2:

$$\frac{\partial}{\partial t}(\rho_2 e_2) + \nabla \cdot (\rho_2 e_2 \mathbf{u}_2) = -\nabla \cdot \mathbf{q}_2 + \rho_2 \dot{q}_{\text{evap,2}} + \rho_2 \dot{q}_{\text{cond,2}} \tag{14}$$

Where:

ρ_2 : Density of Phase 2

$\mathbf{u}_2$: Velocity of Phase 2

p_2 : Pressure of Phase 2

τ_2 : Stress tensor of Phase 2

$\mathbf{F}_{\text{drag,2-1}}$: Drag force on Phase 2 due to Phase 1

e_2 : Internal energy of Phase 2

$\mathbf{q}_2$: Heat flux in Phase 2

$\dot{q}_{\text{evap,2}}$: Evaporation heat transfer rate in Phase 2

$\dot{q}_{\text{cond,2}}$: Condensation heat transfer rate in Phase 2

Non-condensable gases can significantly influence two-phase flows, affecting phase distribution and heat transfer. To account for their presence, a transport equation for the mass fraction of non-condensable gas α_{ncg} can be introduced:

$$\frac{\partial(\rho\alpha_{\text{ncg}})}{\partial t} + \nabla \cdot (\rho\alpha_{\text{ncg}}\mathbf{u}) = S_{\alpha} \tag{15}$$

Where:

ρ : Total density

$\mathbf{u}$: Velocity of the mixture

$S_{\alpha_{\text{ncg}}}$: Source term for non-condensable gas

Closure relations play a critical role in modeling interphase interactions and transfer processes. They are essential to complete the system of equations and make the numerical simulation feasible. The correlations used in the current model include:

Drag Coefficient: The drag force exerted on one phase by another is represented by the drag coefficient $C_{\text{d,1-2}}$. The drag coefficient depends on the flow regime, particle Reynolds number, and

other factors. It can be approximated using empirical correlations such as the Schiller-Naumann equation:

$$C_{\text{d,1-2}} = \frac{24}{Re_{\text{p}}} \left(1 + 0.15 Re_{\text{p}}^{0.687}\right) \tag{16}$$

Where:

Re_{p} : Dispersed Phase Reynolds numbers

For Re_{p} we take the smallest fraction phase between water and vapor presented in the computational cell as the smaller fraction one.

Interfacial Area Density: The interfacial area density a characterizes the total interfacial area per unit volume of the mixture. It is a crucial parameter for modeling interphase mass, momentum, and heat transfer. An empirical correlation to estimate the interfacial area density is the Wen and Yu correlation:

$$a = \frac{C_{\text{WY}}}{d_{\text{p}}} \tag{17}$$

Where:

C_{WY} : Empirical constant

d_{p} : Particle diameter

For d_{p} we take the equivalent cell fraction diameter of the smallest fraction phase between water and vapor presented in the computational cell as the particle one.

Heat Transfer: Heat transfer between phases is a critical aspect of two-phase flows. The Nusselt number (Nu) is commonly used to relate convective heat transfer coefficients to thermal conductivity, providing insights into the rate of heat exchange. For single-phase convective heat transfer, the Nusselt number is defined as:

$$Nu = \frac{hd_P}{k} \tag{18}$$

Where:

h : Convective heat transfer coefficient per flow regime

k : Effective thermal conductivity at the liquid-vapor interface

For the convective heat transfer coefficient we use $Nu = 2$ for modeling interfacial heat exchange across the phases with an elliptic blending based on the volume fraction to mix among both regimes.

Turbulence Modeling: For turbulent flows, accurate modeling of turbulence is essential. Closure relations for turbulent kinetic energy (k) and dissipation rate (ε) are often employed in the context of the Reynolds-averaged Navier-Stokes equations. These equations help quantify the turbulent properties of the flow:

$$\frac{\partial(\rho k)}{\partial t} + \nabla \cdot (\rho k \mathbf{u}) = P_k - \rho\varepsilon + \nabla \cdot [(\mu + \mu_t)\nabla k] \tag{19}$$

$$\frac{\partial(\rho \varepsilon)}{\partial t} + \nabla \cdot (\rho \varepsilon \mathbf{u}) = C_{\varepsilon 1}\frac{\varepsilon}{k}P_k - C_{\varepsilon 2}\rho\frac{\varepsilon^2}{k} + \nabla \cdot [(\mu + \mu_t)\nabla \varepsilon] \tag{20}$$

Where:

P_k : Turbulent production of kinetic energy

$C_{\varepsilon 1}, C_{\varepsilon 2}$: Empirical constants

μ_t : Turbulent viscosity

Phase Change

Closure relations for phase change processes, such as boiling and condensation, involve correlations that account for the heat transfer rates during these transitions. These correlations used consider factors such as nucleation, bubble growth, and film condensation.

Nucleation

Nucleation is the initial step in boiling where vapor bubbles are formed on the heating surface. The nucleation rate (N_{nuc}) can be estimated using the following equation:

$$N_{\text{nuc}} = A_{\text{nuc}} \exp\left(-\frac{B_{\text{nuc}}}{T_{\text{wall}}}\right) \tag{21}$$

Where:

$$A_{\text{nuc}}, B_{\text{nuc}} : \text{Empirical constants}$$

$$T_{\text{wall}} : \text{Wall temperature}$$

After nucleation, bubbles grow in size due to heat transfer. The growth rate (dR/dt) of a bubble with radius R can be approximated by the Rayleigh-Plesset equation:

$$\frac{dR}{dt} = \frac{A_{\text{grow}}}{R}\left(P_{\text{vap}} - P_{\text{sat}}\right) \tag{22}$$

Where:

$$A_{\text{grow}} : \text{Empirical constant}$$

$$P_{\text{vap}} : \text{Vapor pressure}$$

$$P_{\text{sat}} : \text{Saturation pressure}$$

The bubble size is used to update the effective dispersed phase diameter d_P during the computations of the closure models and when the flow regime is undergoing nucleate boiling.

The other two correlations implemented are for bulk boiling heat transfer, which happens at later stages of the evaporator once the flow in the wick has been significantly heated, and film condensation, which is the main mechanism for conversion of the vapor phase into liquid at the evaporator. Note that droplet formation and entertainment is not modeled as a modeling judgment decisions since it is unlikely to appear during condensation in the heat pipe.

Bulk Boiling

The Chen correlation for boiling heat transfer, which reads as follows:

$$\frac{q''}{q''_{\text{max}}} = C_1 \left(\frac{\Delta T}{T_{\text{sat}}} \right)^{n_1} e^{-C_2 (\Delta T / T_{\text{sat}})^{n_2}} \tag{23}$$

Where:

q'' : Heat flux

q''_{max} : Maximum heat flux

C_1, C_2, n_1, n_2 : Empirical constants

ΔT : Temperature difference

T_{sat} : Saturation temperature

Film Condensation

During film condensation, vapor condenses on a cooled surface. The heat transfer rate (q''_{cond}) due to film condensation can be estimated using the Nusselt equation:

$$q''_{\text{cond}} = \frac{k(T_{\text{sat}} - T_{\text{film}})}{L_{\text{film}}} \tag{24}$$

Where:

k : Effective thermal conductivity of the mixture

T_{sat} : Saturation temperature

T_{film} : Film temperature

L_{film} : Characteristic length of the film

We take the characterisitc length of the film as the flooded percentage of the computational cell multiplied by the largest cell length.

The two-phase flow model has been implemented using as the basis the Eulerian Multiphase Model (EMP) in STAR-CCM+. The closure values for the fitting constants can be find in the documentation of the computational code and in the references mentioned for each closure model. Adapted closures are implemented in STAR-CCM+ for nucleate boiling and film condensation

using the previously described models.

Note that in the previous model the capillarity effect of surface tension is not explicitly modeled. This is because explicitly resolving this effect would lead to a prohibitively small mesh in the wick region. To simplify this task, the capillarity force is modeled as an effective volume force canonically computed expressions.

Capillary Force and Volume Force in Wick Structures

To account for the effects of capillarity force in the computational model, it's common to transform the capillary forces into equivalent volume forces. The capillary force (F_{cap}) in a wick is given by the Young-Laplace equation:

$$F_{\text{cap}} = 2\pi r\sigma\cos(\theta) \tag{25}$$

Where:

r : Wick pore radius

σ : Surface tension of the liquid

θ : Contact angle

In the numerical simulation, the curvature pore radius is measured experimentally. Furthermore, we take the standard $\theta = 45^\circ$ for the contact angle in the water wick. To incorporate the capillary effect as a volume force ($\mathbf{F}_{\text{vol}}$) in the computational model, the capillary force can be distributed over the volume of the wick structure. The volume force can then be computed as:

$$\mathbf{F}_{\text{vol}} = \frac{F_{\text{cap}}}{A_{\text{cap}} L_{\text{wick}}}\mathbf{e}_z \tag{26}$$

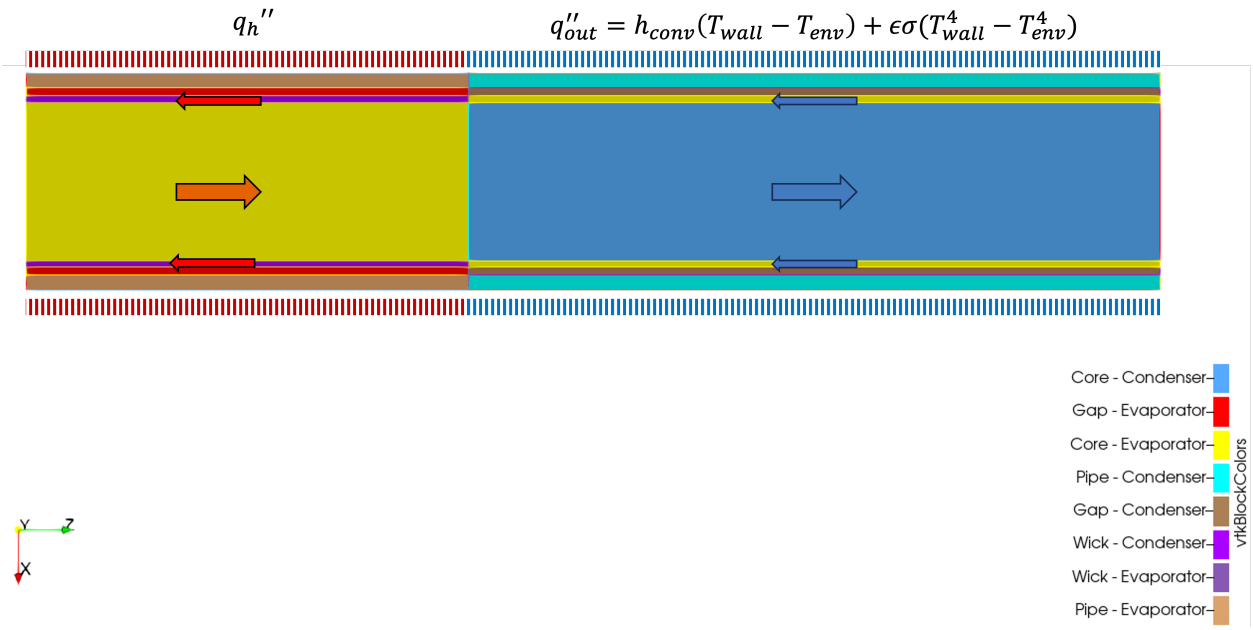

Figure 1: Domain for the CFD simulations with the labels for each part of the domain. The arrows show the fluid circulation in the pipe and the azimuth-symmetric boundary conditions are specified in the figure. Note: the pipe dimension has been scaled by a factor of 0.05 in the axial direction for visualization purposes.

Where:

L_{wick} : Length of the wick

A_{cap} : Cross-sectional area of the wick's capillary section

$\mathbf{e}_z$: Unit vector in the wick direction

For completeness, the domain and boundary conditions for the two-phase CFD model are presented in Figure 1. Four key regions are modeled for the evaporator and condenser: core, wick, pipe, and gap between the wick and the pipe. The flow field is modeled only in the core and wick region. The gap integrates surface-to-surface radiation heat transfer models, while the pipe integrates a heat conduction model. A uniform heating (q''_h) is applied to the outer wall of the copper pipe at the evaporator, whereas convective and free-radiation ($q''_{out} = h_{conv}(T_{wall} - T_{env}) + \epsilon\sigma_{SB}(T^4_{wall} - T^4_{env})$, where T_{env} is the environment temperature measured in the experiment, ϵ is the pipe's emissivity, and σ_{SB} is the Stefan–Boltzmann constant) heat transfer boundary conditions to the room temperature are applied at the pipe's wall in the condenser region.

4. Results of the modeling

The forthcoming section is bifurcated into two distinct components. Initially, a comparative scrutiny is undertaken, pitting the conduction and two-phase models against the experimental data meticulously acquired by Katrina Sweetland, meticulously documented within her Ph.D. manuscript [8]. Only single evaporator-condenser models are compared against the results presented in this dissertation. This analytical endeavor is poised to yield a comprehensive evaluation of the anticipated efficacy of the equivalent heat conduction and two-phase flow model in the context of unblemished wall temperatures. This analytical undertaking constitutes a salient milestone within the purview of this research inquiry. Subsequently, the latter segment of this results section entails a rigorous dissection of the computational fluid dynamics (CFD) modeling outcomes, with the goal of attaining a more profound and quantifiable elucidation of the operational dynamics intrinsic to the heat pipes under consideration.

4.1 Description of the experiment

The copper-liquid heat pipe under investigation features a specially designed wick structure fabricated from a tightly rolled copper grid over a mandrel. This design promotes efficient capillary action within the wick, enhancing the overall heat transfer efficiency. Notably, the heat pipe is equipped with the ability to control its internal gas pressure, offering the flexibility to manage the presence of non-condensable gases within the system. The combination of the tailored wick structure and gas pressure control contributes to the enhanced thermal performance of the heat pipe. The parameters specifying the heat pipe design are the following e:

- The length of the evaporator section, denoted as $length_{evap}$, is calculated to be 0.78 m. This segment of the heat pipe initiates the vaporization process as the working fluid absorbs heat from its surroundings.
- The length of the condensation section is determined as 1.22 m. This segment facilitates the heat release from the vapor as it undergoes phase change and condenses back into a liquid state.
- Outer diameter of the clad, D_{clad_o}, is 19.1 mm. This parameter contributes to the overall heat

pipe dimensions and influences the heat transfer process.

- Inner diameter of the clad, D_{clad_i}, is 16.5 mm. This parameter, in conjunction with the outer diameter, determines the thickness of the heat pipe's wall, affecting its heat conduction characteristics.

- Outer diameter of the wick, D_{wick_o}, is 15.1 mm. The wick's outer diameter plays a crucial role in determining the capillary action efficiency within the heat pipe.

- Inner diameter of the wick, D_{wick_i}, is 14.0 mm. This parameter, combined with the outer wick diameter, defines the wick's geometry and its capillary pumping potential.

- Pore radius of the heat pipe, R_{pore}, is 75 micrometers. The pore radius influences capillary flow resistance within the wick and significantly affects the overall heat pipe performance. A nonhomoegenous distribution of pore diameters was observed in the characterization experiments of the heat pipe. However, as a full characterization has not been measured, we take the porous radius as constant over the wick.

The experiment initiates with the heat pipe at an initial temperature of 296 K. This value serves as the baseline temperature for the heat transfer process within the heat pipe and is assumed as the external room temperature. The surrounding ambient environment contributes a convective heat transfer coefficient of 5 W/(m²·K), signifying the interaction between the heat pipe and its external surroundings. Additionally, the heat pipe's surface emissivity is determined to be 0.796, indicating the condenser material's ability to radiate heat energy. Both the convective and radiation heat transfer define an effective convection coefficient of $\sim$15 W/(m²·K). However, in the present models, both convection and radiation at the wall of the condenser are separately modeled. Surface-to-surface radiation heat transfer is included in the two-phase model at the gap region. The emissivity is taken to be 0.796 also for the internal gap.

For the wall temperature measurements, 31 thermocouples are placed over the heat pipe wall with an approximately equidistant space. In this work we compare our results with 15 out of the 31 placed thermocouples for simplicity. The positions of the thermocouples will be indicated in the results section. We refer the reader to the manuscript [8] for further information and documentation about the experiment.

4.2 Comparison of wall temperatures between the numerical models and experimentally measured values

In this first study, a comparative analysis of heat pipe performance is conducted, with a focus on the absence of non-condensable gases. The experimental data is compared with simulation results, providing valuable insights into the thermal behavior of the system. Figure 2 showcases the results of this investigation.

The experimental protocol involves subjecting the heat pipe to a uniform power input at the evaporator for a duration of 1 hour, totaling 65 W. Subsequently, the heating source is deactivated, and the heat pipe is allowed to cool down naturally. This controlled experiment serves as a basis for evaluating the effectiveness of both conduction and two-phase Computational Fluid Dynamics (CFD) models.

The comparative analysis reveals a noteworthy qualitative agreement between the experimental and modeled outcomes. Both the conduction and two-phase CFD models demonstrate their potential to predict the heat pipe's thermal dynamics. However, a distinct disparity is observed in the axial effective conductivity predicted by the conduction model. This leads to a narrower temperature spread in comparison to the experimental observations.

The observed discrepancy in the conduction model's predictions is attributed to its inability to capture the intricate local flow dynamics within the heat pipe's core. This phenomenon ultimately results in the evaporation section of the heat pipe attaining significantly higher temperatures than the rest of the system. Notably, the two-phase CFD model effectively captures this intricate flow behavior and appropriately predicts this distinctive thermal behavior. Additionally, this test involved partial dryout at the evaporator, which explains the large temperature observed for the towards the left of the pipe. This phenomenon is appropriately captured by the CFD model, while is evidently not captured in the heat conduction model as it breaks the fundamental modeling hyoitheses of this one.

It is noteworthy that despite its simplified approximations, the heat conduction model still offers reasonable predictions. Its qualitative agreement with experimental results underscores the utility of such simplified models in preliminary assessments of heat pipe performance.

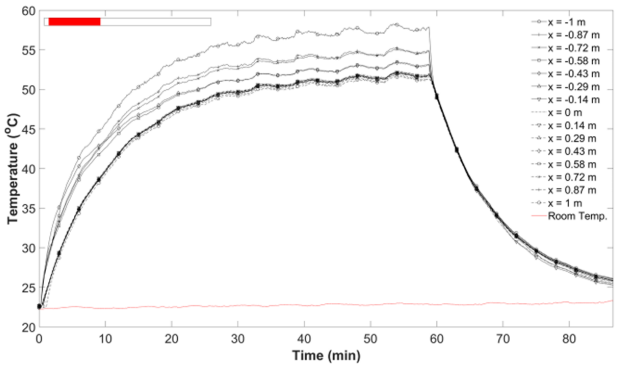

(a) Experimental Results.

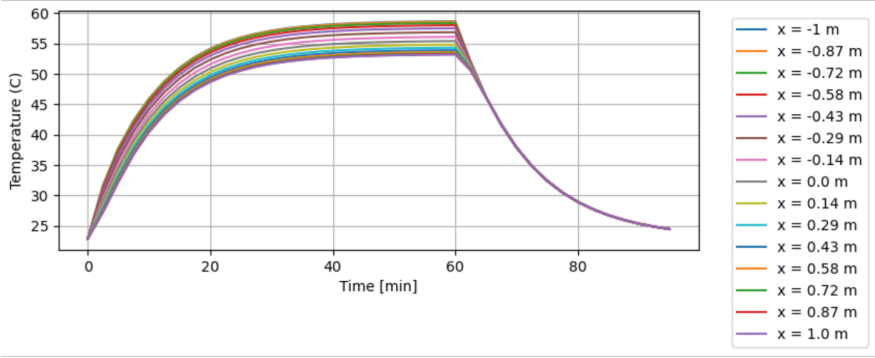

(b) Results Obtained by the Heat Conduction Calculations.

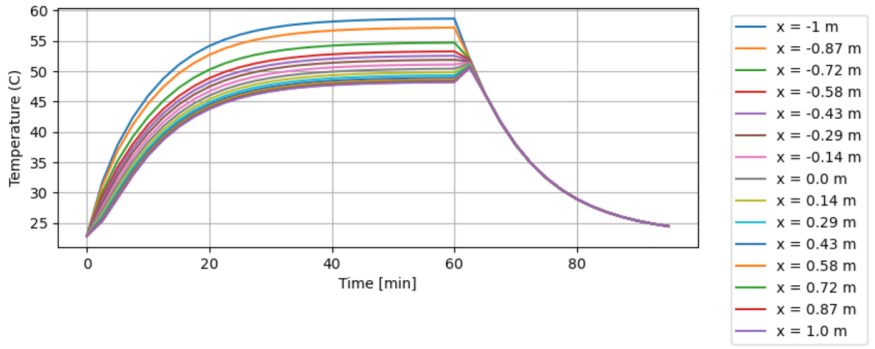

(c) Results Obtained by the two-phase CFD Calculations.

Figure 2: Results for the experiments without using non-condensable gases.

The investigation proceeds with a thorough assessment of the influence of non-condensable gases on heat pipe performance. The outcomes of this analysis are depicted in Figure 2, offering insights into the interaction between non-condensable gases and the heat pipe's thermal dynamics.

The experimental procedure involves controlled introduction of non-condensable gases into the heat pipe environment. The heat pipe is subjected to a consistent 1-hour heating phase, with a uniform power input of 75 W at the condenser. Subsequently, the heat pipe undergoes a natural cooling phase.

Both the conduction model and the two-phase CFD model demonstrate consistent qualitative agreement with the experimental findings. This alignment underscores the predictive capabilities of both models in simulating the complex thermal behavior of the heat pipe.

A noteworthy observation emerges: thermocouples near the condenser's terminal—where non-condensable gases accumulate—exhibit lower temperatures. This phenomenon is accurately replicated by both models, validating their predictive capacity in capturing the heat pipe's thermal dynamics.

The conduction model's precision hinges on an input parameter: the estimated length of the non-condensable section in the condenser. This calibration factor contributes to the model's capacity to closely align with experimental findings.

As non-condensable gases migrate towards the condenser's end, a distinct thermal interplay arises—a result of heating and cooling dynamics introduced by the gases. The CFD model adeptly reproduces this interaction, showcasing its capability to simulate non-condensable gas effects.

However, a subtle deviation surfaces regarding the last thermocouple before the non-condensable gas section. The CFD model's temperature prediction exhibits a slight disparity—a potential overestimation of the gas section's extent, impacting the thermocouple's reading.

Nevertheless, the broader agreement between the CFD model and experimental data remains steadfast and enlightening. The fusion of numerical simulations and experimental exploration yields insights into the intricate thermal dynamics influenced by non-condensable gases within the heat pipe system.

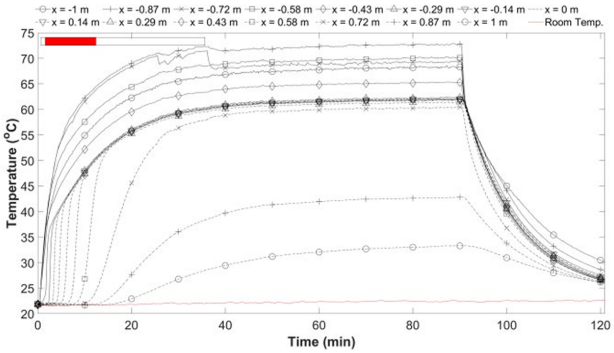

(a) Experimental Results.

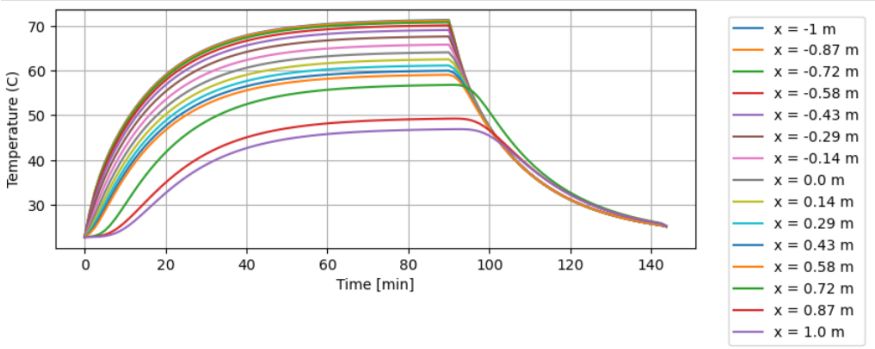

(b) Results Obtained by the Heat Conduction Calculations.

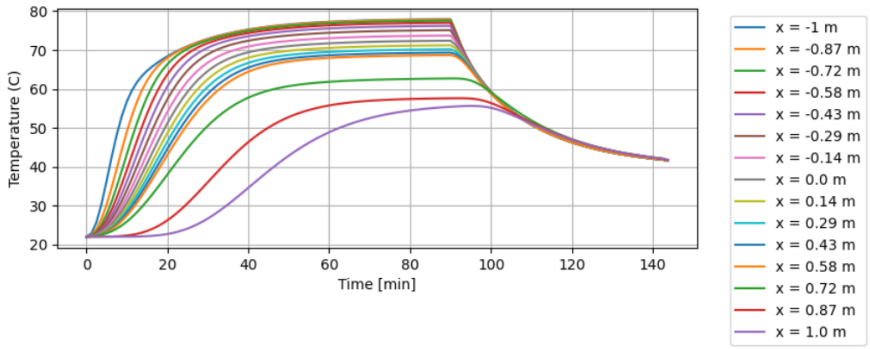

(c) Results Obtained by the two-phase CFD Calculations.

Figure 3: Results for the experiments with non-condensable gases in the heat pipe.

In summary, this section demonstrates a strong agreement between the conduction and CFD models when compared to transient experimental measurements of wall temperatures. Both models successfully predict the heat pipe's start-up and shutdown dynamics. However, a more pronounced concurrence is observed in the dynamics projected by the CFD model compared to

the conduction model. The main reason for this disparity is that the conduction model assumes a canonical flow inside the heat pipe. Nevertheless, we will later establish, through CFD numerical simulations, that this flow may not be canonical, leading to expected disparities in the conduction model's predictions.

For comprehensive analysis, the experimental data has been digitized, and the average numerical errors in relation to the experiments have been computed for all thermocouples and across time. These errors are presented in Table 1. As anticipated, the conduction model exhibits larger errors compared to the CFD model, and for both scenarios, the errors slightly increase when non-condensable gases are introduced. Nevertheless, the observed differences remain within acceptable limits in line with the models' anticipated behavior.

Importantly, it is worth noting that the effective conduction model's runtime is approximately 10^3 times faster than that of the CFD model. Hence, these models are preferred when utilizing heat pipes for nuclear reactor modeling.

Table 1: Temperature Discrepancies (in Kelvin) - Conduction and CFD Two-Phase Model vs. Experiments

	Conduction Model	CFD Two-Phase Model
Without Non-Condensables	3.7	0.9
With Non-Condensables	5.4	1.7

4.3 Key results of the 2-phase Computational Fluid Dynamics analyses

This section presents key outcomes from the CFD studies, contributing to a comprehensive understanding of the heat pipe's behavior. It is important to highlight that the CFD mesh has been meticulously refined to achieve mesh independence for these results. The resulting meshes encompass approximately 23 million elements.

For clarity and simplicity, we exclusively present outcomes related to the steady-state operation of the heat pipe. This focused approach provides a clear lens through which to examine the system's behavior within the context of sustained operation.

The mass fluxes for vapor and liquid within heat pipes operating both with and without non-

condensable gases are depicted in Figure 4. As anticipated, vapor mass fluxes coalesce at the heat pipe's core, engaging in a circulation pattern from left to right (evaporator to condenser), whereas liquid mass fluxes amass at the wick and follow a circulation route from condenser to evaporator.

Notably, negligible interaction between the vapor core and the liquid phase is observed within the evaporator region. A distinct liquid stagnation point materializes at the condenser's extremity, attributed to the accumulation of liquid originating from the wick. Experimental observations align with this phenomenon, substantiating the presence of this liquid plug at the pipe's terminus [8].

In the domain of the condenser, a discernible interplay between the liquid phase and the vapor transpires within the pipe's interior. This phenomenon stems from the condensation of vapor, subsequently leading to liquid accumulation in the condenser region. The resultant solidification of liquid prompts its directed migration to the wick.

Significantly, the numerical simulation unveils disparate transport mechanisms for liquid in heat pipes, contingent upon the presence or absence of non-condensable gases. In heat pipes devoid of non-condensable gases, minute liquid bodies emerge at the condenser, induced by liquid-vapor surface tension, rapidly channeled towards the wick.

Conversely, heat pipes with condensable gases are characterized by a distinct interplay. The compression and subsequent expansion of non-condensable gases situated at the heat pipe's end yield upstream pressure waves, serving as nucleation sites for multiple liquid bodies. This intricate phenomenon aids the coalescence of minute liquid bodies within the condenser, culminating in the formation of more substantial liquid masses.

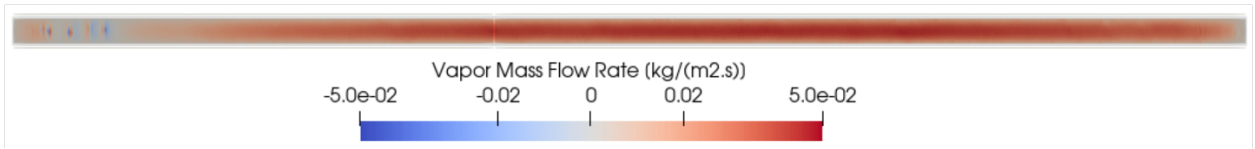

(a) Vapor Mass Flux Without Non-Condensables

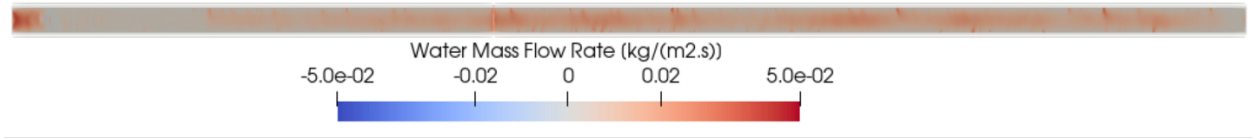

(b) Liquid Mass Flux Without Non-Condensables

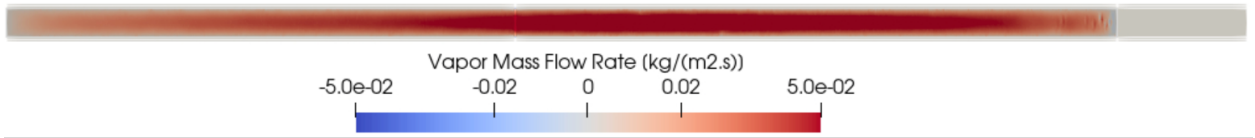

(c) Vapor Mass Flux With Non-Condensables

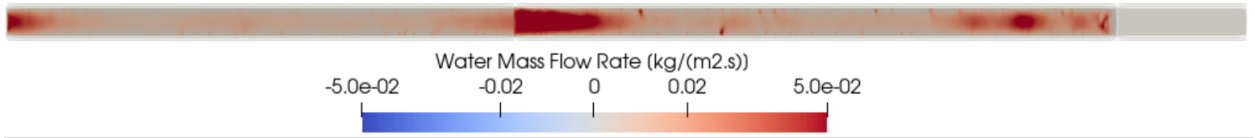

(d) Liquid Mass Flux With Non-Condensables

Figure 4: Comparison of the mass flux profiles for the extracted liquid and vapor in the heat pipe during nominal operation conditions once the heat pipe reaches steady state.

A more profound comprehension of the liquid transport mechanism within the heat pipe is attained through an intricate scrutiny of both the evaporator and condenser sections. The mass fluxes of liquid within the mid-section of the evaporator and condenser—pertaining to heat pipes with and without non-condensable gases—are presented in Figure 5.

An intricate interplay emerges between the liquid conveyed by the wick and the vapor flow at the core of the pipe, a phenomenon observed in both scenarios. Within zones characterized by varying pressures, the vapor either draws or propels the liquid flow towards the wick. At the evaporator, vapor generated within the wick propels into the core of the pipe. This projected vapor jet behavior diverges from the spatially uniform vapor generation rate postulated in the conduction model. Moreover, these vapor jets entrain small quantities of liquid into the vapor core, thereby causing a fraction of the evaporation to transpire within the vapor core, influenced by the interaction between the entrained liquid and the warmer vapor.

The dynamic unfolds somewhat similarly at the condenser in cases involving non-condensable gases. Minute liquid bodies generated at the condenser are propelled towards the wick, subsequently propelled by the forthcoming wick flow and capillary pressure. In contrast, the pipe featuring non-condensable gases experiences a more gradual dynamic, as larger liquid masses form, gradually diffusing towards the wick.

It is pertinent to note that, in both scenarios, the entrainment of liquid into the wick constitutes a marginal fraction of the vapor condensing within the wick region—an anticipated operational mechanism of the heat pipe. However, as previously observed, these phenomena hold significance enough to induce deviations from the performance presumptions of conduction models.

The temperature profiles for vapor and liquid within heat pipes—both with and without non-condensable gases—are portrayed in Figure 6. These temperature profiles comport themselves in a manner consistent with expectations.

Vapor undergoes heating at the evaporator and subsequently traverses the core of the pipe, coursing towards the condenser. Upon entering the condenser region, vapor experiences a deceleration as portions of it begin to condense in proximity to the wick. Subsequently, beyond a specific juncture, the remaining vapor experiences a sudden condensation event.

Notably, this behavior might be attributed to the numerical approximations governing film boiling, encompassing a condensing mass flux potentially overestimated for the rarified vapor gas

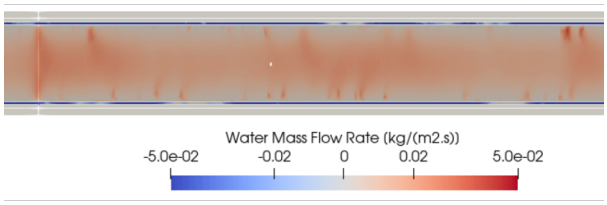

(a) Detailed of Liquid Mass Flux in Evaporator Without Non-Condensables

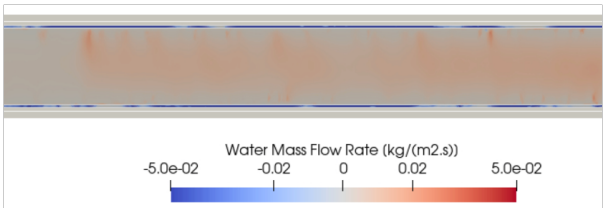

(b) Detailed of Liquid Mass Flux in Condenser Without Non-Condensables

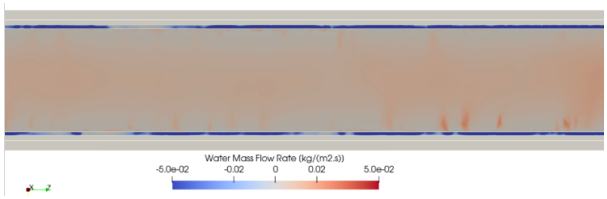

(c) Detailed of Liquid Mass Flux in Evaporator With Non-Condensables

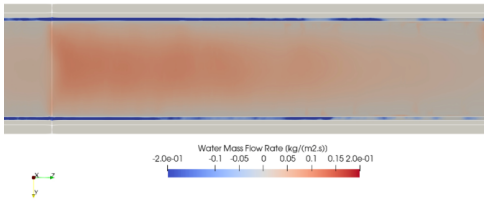

(d) Detailed of Liquid Mass Flux in Condenser With Non-Condensables

Figure 5: Detailed Liquid Mass Flux at mid-section of evaporator and condenser with and without non-condensable gases.

situated towards the condenser's end. The pipes, irrespective of non-condensable gas presence, exhibit comparable behavior as the vapor approaches the effective end of the condenser.

The temperature of the non-condensable gas amassed at the heat pipe's terminus remains consistently stable. Concurrently, the temperature of liquid increases concomitant with its circulation downstream the wick, a phenomenon anticipated.

It is evident that the temperature of liquid entrained within the pipe's core registers lower than the surrounding vapor. This is an anticipated outcome, as this entrained liquid originates from the internal portion of the wick—a sector, which necessitates a substantially lengthier interval to attain elevated temperatures compared to the external region.

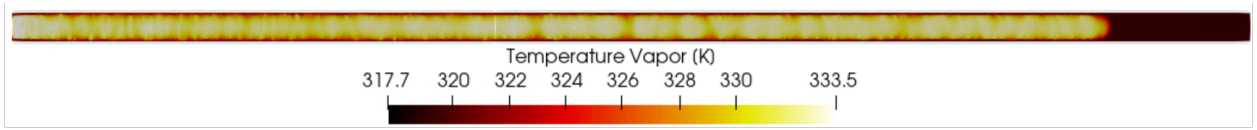

(a) Vapor Temperature Without Non-Condensables

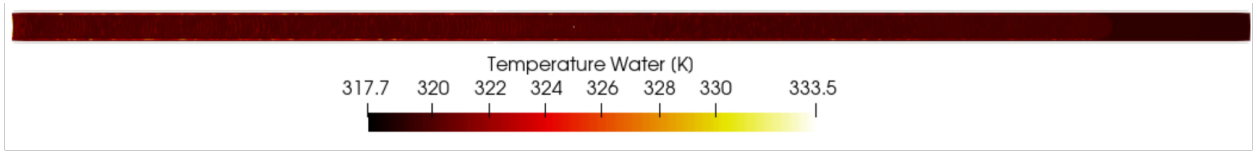

(b) Liquid Temperature Without Non-Condensables

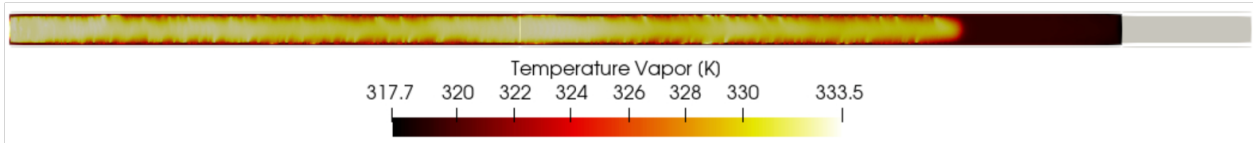

(c) Vapor Temperature With Non-Condensables

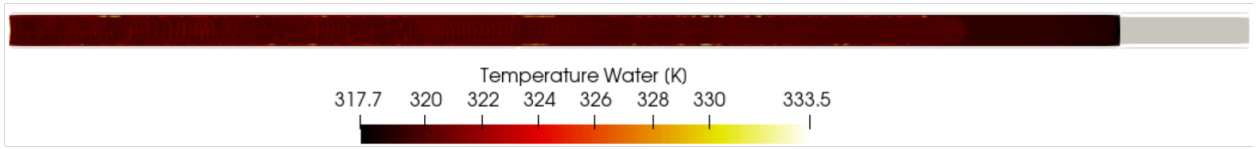

(d) Liquid Temperature With Non-Condensables

Figure 6: Comparison of the temperature profiles for the extracted liquid and vapor in the heat pipe during nominal operation conditions once the heat pipe reaches steady state.

The thresholded volume fractions of liquid and vapor, colored by the vorticity magnitude, are presented for both pipes—those with and without non-condensable gases—in Figure **??**. As observed earlier, liquid flow within the wick undergoes a non-continuous pattern, attributed to the evaporating liquid propelling into the core, and the liquid bodies formed within the bulk of the condenser being directed towards the wick.

In stark contrast, the vapor phase evinces notably higher continuity. Liquid exhibits elevated vorticity magnitudes at locations where the wick interacts with the vapor core flow. Beyond this, the vorticity profile of liquid assumes a relatively uniform distribution. For vapor, the vorticity dynamics differ between the pipe without non-condensable gases and its counterpart.

While the vorticity profile for the pipe with non-condensable gases remains relatively flat, distinct spikes are evident for the counterpart pipe featuring non-condensable gases. Subsequent exploration unveiled that these pronounced vorticity points in the latter scenario align with elevated pressure zones within the condenser. These pressure-driven phenomena prompt the nucleation of multiple liquid bodies. The consequence of this behavior manifests as heightened mixing within the vapor phase, ultimately culminating in increased vorticity within these designated regions.

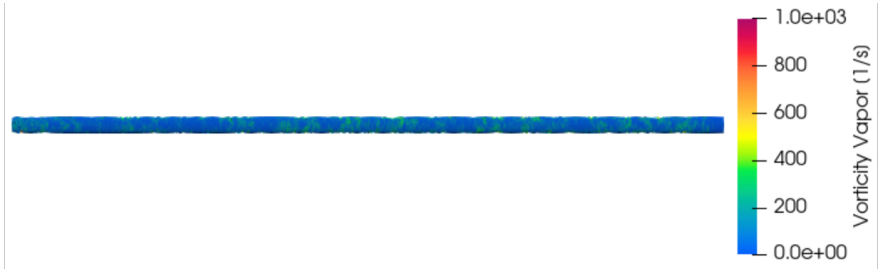

(a) Vapor Vorticity Without Non-Condensables

(b) Liquid Vorticity Without Non-Condensables

(c) Vapor Vorticity With Non-Condensables

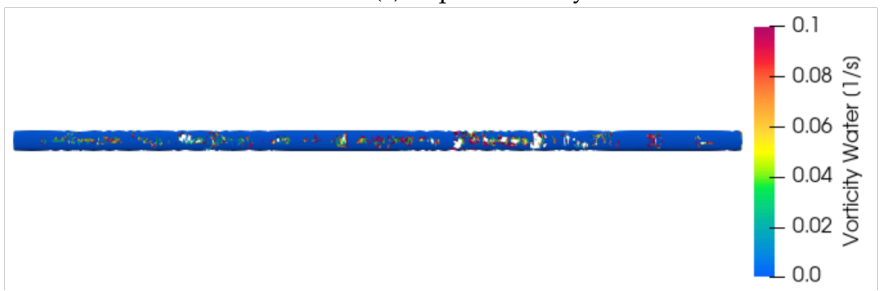

(d) Liquid Vorticity With Non-Condensables

Figure 7: Comparison of the vorticity profiles for the extracted liquid and vapor in the heat pipe during nominal operation conditions once the heat pipe reaches steady state.

In summary, this section has demonstrated the predicted behavior of the heat pipe through more detailed two-phase CFD simulations. In particular, the main phenomena observed coincides with the assumptions of the conduction model. This could be the reason why the conduction model shows a relatively good agreement with experimental data. Additionally, this heat pipe has a copper wall, so the conduction effect may hinder some of the diffusion or core-wick interaction effect. Nonetheless, some second-order phenomena not included in the standard conduction model have been observed. These phenomena are related to the jet-like mixing interaction between the wick and the core flow, as well as the non-uniform core pressure field generated by the non-condensable gases. The better agreement of the CFD simulations with experimental data suggests that these phenomena should be integrated into the conduction models in the future. However, further investigation is needed to confirm the accuracy of the flow phenomena observed in the CFD models.

5. Summary

This summary presents a comprehensive overview of the insights and findings derived from a detailed discussion on the conduction model and two-phase Euler-Euler models in Computational Fluid Dynamics (CFD), as applied to heat pipes, and their comparison against experimental data for heat pipes with and without non-condensable gases. The report covers various aspects of the development of the conduction and two-phase CFD models, including modeling equations, closure relations, energy conservation, nucleation, bubble growth, film condensation, non-condensable gases, and heat pipe behavior analysis. Additionally, within the expected modeling uncertainties, we have validated both the CFD and conduction models against experimental data [8].

Since, to our knowledge, this is the first time that a complete two-phase Euler-Euler CFD model has been developed to study heat pipes, we pay further attention to this model. We observe that the two-phase Euler-Euler model is a vital framework in CFD for simulating heat pipes. It comprises mass, momentum, and energy conservation equations for both vapor and liquid phases, without the bulk homogenizing hypotheses that reduce the accuracy of the models. Closure relations, including interfacial drag and intra-phase turbulence, govern phase interaction. Energy conservation equations encompass heat transfer through conduction, convection, and phase change.

A more detailed model was necessary to capture the evaporator dynamics and achieve a better comparison to experimental data. This model involves a separate treatment for nuclear vapor growth dynamics and bulk boiling. Additionally, only film boiling is considered in the condenser. Nonetheless, film condensation on a wick's surface is influenced by temperature gradients and vapor-liquid interactions, which challenge the uniform film condensation hypothesis. Hence, improved models will be required as this research progresses.

According to our numerical studies, the introduction of non-condensable gases impacts heat pipe behavior beyond reducing the active length of the condenser. These gases influence pressure dynamics and affect heat transfer. The modeling of non-condensable gases involves transport equations for their concentration. This is particularly important for predicting the start-up dynamics of the pipe, but during nominal operation, non-condensable gases simply accumulate

towards the end of the condenser.

These 2D and 3D effects are of interest for both heat pipes configuration with and without non-condensable gas. Internal injection and suction alter the velocity profile and has not been widely studied since the mid to late 80's (Busse and Haug [9]). The suction in the condenser has a very strong influence on the velocity and pressure of the vapor, adding gas tends to amplify this as the shorter effective condenser may increase the radial Reynolds number. This studies could be perform in further details using CFD models as has been shown in this work.

Comparing experimental data with CFD simulations reveals insights. Steady-state operation unveils the heat pipe's behavior, with both models offering qualitative alignment. However, nuances observed in CFD, such as vapor jets and water entrainment, highlight the distinctions between the models. A detailed analysis of water transport mechanisms showcases intricate interactions between the wick and vapor. Vorticity magnitude studies indicate mixing behavior, with pronounced vorticity spikes observed in certain scenarios.

Further research is needed to gain a better understanding of how these liquid-gas interactions may impact heat pipe performance. This enhanced understanding will ultimately lead to improved numerical models of heat pipes, potentially reducing the reliance on extensive experimentation.

This scientific exchange's novelty delves into the nuanced world of two-phase CFD modeling for heat pipes. The insights garnered reveal the convergence and divergence of CFD and conduction models, the role of non-condensable gases, and intricate transport mechanisms. These findings underscore the evolving landscape of heat pipe simulations and highlight the importance of continuous investigation and integration of real-world phenomena into models.

REFERENCES

[1] A. Rohani and C. Tien, "Steady two-dimensional heat and mass transfer in the vapor-gas region of a gas-loaded heat pipe," *Journal of Heat Transfer*, vol. 95, pp. 377–382, 1973.

[2] P. Prado-Montes, D. Mishkinis, A. Kulakov, A. Torres, and I. Pérez-Grande, "Effects of non condensable gas in an ammonia loop heat pipe operating up to 125° c," *Applied thermal engineering*, vol. 66, no. 1-2, pp. 474–484, 2014.

[3] J. Huang, J. Zhang, and L. Wang, "Review of vapor condensation heat and mass transfer in the presence of non-condensable gas," *Applied thermal engineering*, vol. 89, pp. 469–484, 2015.

[4] C. W. Lee, J.-S. Yoo, and H. K. Cho, "Multi-scale simulation of wall film condensation in the presence of non-condensable gases using heat structure-coupled cfd and system analysis codes," *Nuclear Engineering and Technology*, vol. 53, no. 8, pp. 2488–2498, 2021.

[5] K. Kekaula, Y. Cheng, Y. Chen, T. Ma, and Q. Wang, "Computational fluid dynamics modeling of steam condensation in the presence of noncondensable gas in inclined tubes," *Heat Transfer Engineering*, no. just-accepted, pp. 1–13, 2023.

[6] H. Sun, M. Pellegrini, C. Wang, S. Suzuki, K. Okamoto, W. Tian, S. Qiu, and G. Su, "Cfd simulation based on film model of high temperature potassium heat pipe at different positions: Horizontal, vertical, and 45° inclined," *Progress in Nuclear Energy*, vol. 154, p. 104442, 2022.

[7] X. Wang, Y. Shi, T. Liu, S. Wang, K. Wang, H. Chen, Y. Wang, and Y. Zhu, "Cfd modeling of liquid-metal heat pipe and hydrogen inactivation simulation," *International Journal of Heat and Mass Transfer*, vol. 199, p. 123490, 2022.

[8] K. Sweetland, "Heat pipes with arbitrary boundary conditions," 2022.

[9] C. Busse and J. Kemme, "Dry-out phenomena in gravity-assist heat pipes with capillary flow," *International Journal of Heat and Mass Transfer*, vol. 23, no. 5, pp. 643–654, 1980.